Chapter 13
Theoretical and Experimental Analysis of Bifurcation Induced Passive Bandgap Reconfiguration

Michael J. Mazzoleni, Brian P. Bernard, Nicolas Garraud, David P. Arnold, and Brian P. Mann

Abstract This paper presents a theoretical analysis and experimental validation of passively reconfigurable bandgaps in a 1D chain of oscillators. Nonlinearities in the system result in a morphing of the bandgap structure when the excitation amplitude passes a certain threshold. Specifically, an asymmetric bistability is used to achieve amplitude dependent filtering through passive bandgap reconfiguration. The experimental system consists of a 1D chain of axially aligned pendulums arranged in dimer unit cells with nearest neighbor coupling. Repulsive magnets are used to induce bistability in the pendulums. Comparisons between experiments and theory show good agreement.

Keywords Vibrations • Wave propagation • Bandgaps • Bifurcations • Bistability

13.1 Introduction

Wave propagation through periodic structures is a phenomenon of interest in mechanical, photonic, and electrical systems [1–3]. The study of wave propagation behavior in periodic structures has led to significant advances in signal processing, wave guiding, and vibration absorption technologies [4]. Periodic structures typically exhibit two fundamental modes: propagation and attenuation [5, 6]. In recent years, there has been significant interest in the design and development of metamaterials that have desirable wave propagation characteristics. One of the primary focuses of these studies is the manipulation of bandgaps in periodic structures.

Bandgaps are attenuation zones that exist between two propagation zones, and it is often desirable to tune these bandgaps for specific applications. Currently, there are two main approaches for tuning bandgap behavior. The first approach is based on design methodologies and utilizes careful selection of material properties and geometries [7–10]. However, once designed, the bandgap structures of these systems are fixed. The second approach is based on active control and tunes the bandgap behavior through component replacements, variable adjustments, and manual switching [11–14]. This approach enables the bandgap structure to reconfigure itself, but it requires human intervention and is not suitable for autonomous operation.

This paper builds upon previous studies conducted by the authors and presents a method for achieving passive bandgap reconfiguration, which enables the bandgap structure to alter its wave propagation characteristics in response to its environment [15, 16]. Therefore, this system is autonomous and adaptable. The system described in this paper achieves amplitude dependent filtering, which allows waves of a given frequency to propagate below a certain amplitude threshold. However, once the amplitude crosses that threshold, a bifurcation occurs and the waves are attenuated. A theoretical model is presented to explain this phenomenon, and an experimental setup is used to validate the model.

M.J. Mazzoleni (✉) • B.P. Mann
Dynamical Systems Laboratory, Department of Mechanical Engineering and Materials Science, Duke University, Durham, NC 27708, USA
e-mail: michael.mazzoleni@duke.edu; brian.mann@duke.edu

B.P. Bernard
Autonomous Systems Laboratory, Department of Mathematics, Schreiner University, Kerrville, TX 78028, USA
e-mail: bpbernard@schreiner.edu

N. Garraud • D.P. Arnold
Interdisciplinary Microsystems Group, Department of Electrical and Computer Engineering, University of Florida, Gainesville, FL 32611, USA
e-mail: darnold@ufl.edu

G. Kerschen (ed.), *Nonlinear Dynamics, Volume 1*, Conference Proceedings of the Society for Experimental Mechanics Series, DOI 10.1007/978-3-319-15221-9_13

13.2 Math Model

This section presents a mathematical model that describes the wave propagation characteristics of a 1D array of axially aligned pendulums. The pendulum array consists of repeating dimer unit cells consisting of two pendulums, and each pendulum is torsionally coupled to its neighbors. A schematic of this pendulum system is shown in Fig. 13.1. The system's bandgap regions are calculated by applying periodic boundary conditions to the system, assuming a traveling wave solution, and solving the resulting eigenvalue problem. Reconfigurable bandgaps are made possible by introducing bistability into the system through a nonlinear restoring torque. If the bistability is asymmetric, then the system will have two distinct bandgap profiles.

13.2.1 Equations of Motion

Consider a unit cell of the pendulum array which consists of two coupled pendulums with periodic boundary conditions and with a nonlinear restoring torque $f(\theta_2)$ applied to the second pendulum. The pendulums are assumed to be rods which each have a lumped mass added to them. The system will only exhibit a bandgap region when these masses are different. A homogeneous unit cell will result in a system with no bandgaps. The governing equations of motion for this system are

$$I\ddot{\theta}_1 + \left(\epsilon m_1 + \frac{m}{2}\right) gL \sin\theta_1 + 2k\left(\theta_1 - \theta_2\right) = 0, \tag{13.1}$$

$$I\ddot{\theta}_2 + \left(\epsilon m_2 + \frac{m}{2}\right) gL \sin\theta_2 + 2k\left(\theta_2 - \theta_1\right) + f\left(\theta_2\right) = 0, \tag{13.2}$$

where θ_j is the angular displacement of the jth pendulum, I is the mass moment of inertia of each pendulum, L is the length of each pendulum, ϵ is the ratio of the location of the added mass vs. the length of each pendulum rod, m is the mass of each pendulum rod, k is the linear torsional coupling constant between any two adjacent pendulums, g is the acceleration due to gravity, and m_j is the mass added to the jth pendulum. If $\epsilon = 1$, then the masses m_j are located at the tips of the pendulum rods. For convenience, the dimensionless time variable $\tau = t\sqrt{g/L}$ can be introduced and Eqs. (13.1) and (13.2) can be rewritten in dimensionless form as

$$\theta_1'' + \eta \sin\theta_1 + \kappa_1\left(\theta_1 - \theta_2\right) = 0, \tag{13.3}$$

$$\theta_2'' + \mu \sin\theta_2 + \kappa_2\left(\theta_2 - \theta_1\right) + F\left(\theta_2\right) = 0, \tag{13.4}$$

where $\theta_j'' = d^2\theta_j/d\tau^2 = \ddot{\theta}_j L/g$, $\eta = \left(6\epsilon\alpha + 3\right)/\left(6\epsilon^2\alpha + 2\right)$, $\mu = \left(6\epsilon\beta + 3\right)/\left(6\epsilon^2\beta + 2\right)$, $\kappa_1 = 6\kappa/\left(3\epsilon^2\alpha + 1\right)$, $\kappa_2 = 6\kappa/\left(3\epsilon^2\beta + 1\right)$, $F\left(\theta_2\right) = 3f\left(\theta_2\right)/\left(3\epsilon^2\beta + 1\right)mgL$, $\alpha = m_1/m$, $\beta = m_2/m$, and $\kappa = k/mgL$.

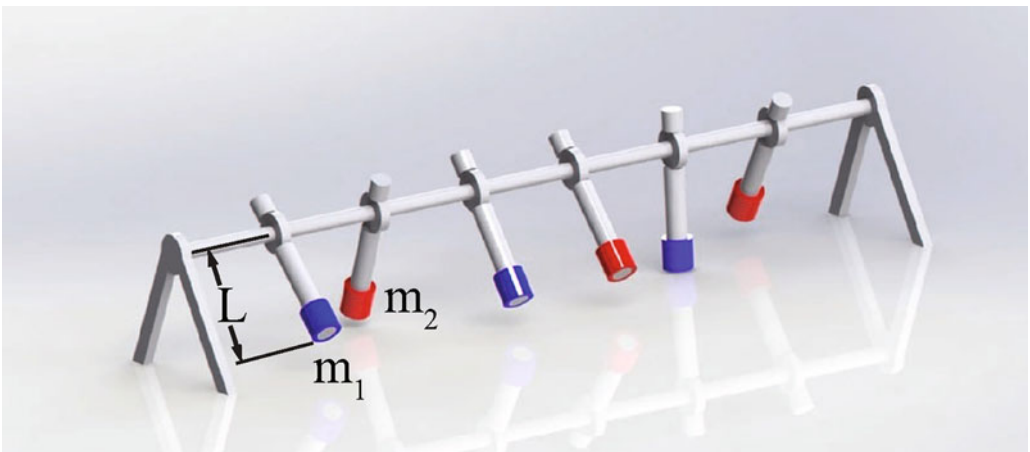

Fig. 13.1 Schematic of a 1D array of axially aligned pendulums. The pendulums are assumed to be rods of length L which each have a lumped mass added to them. Each unit cell consists of two pendulums, and the masses can differ between the two pendulums

13.2.2 Bandgap Calculations

To determine the system's bandgap structure, a traveling wave solution can be assumed in the form

$$\theta_j = A_j e^{i(j\gamma - \tilde{\omega}\tau)}, \tag{13.5}$$

where A_j is the amplitude of the jth pendulum's oscillations, γ is the wavenumber, and $\tilde{\omega}$ is the dimensionless propagation frequency. A standard eigenvalue problem can be formulated by substituting Eq. (13.5) into Eqs. (13.3) and (13.4) and then linearizing the system about an equilibrium, resulting in

$$\left[S(\gamma) - \tilde{\omega}^2 I\right] A = 0, \tag{13.6}$$

where

$$S(\gamma) = \begin{bmatrix} \kappa_1 + \eta & -\kappa_1 \cos\gamma \\ -\kappa_2 \cos\gamma & \kappa_2 + \mu + \sigma \end{bmatrix}, \tag{13.7}$$

and σ is the linearized value of $F(\theta_2)$ for a given equilibrium. Equation (13.6) can then be solved to construct the bandgap structure of the system. For bandgap calculations, it is only necessary to consider values of γ within the first Brillouin zone [17]. Therefore, the reduced wavenumber γN should be varied from 0 to π, where $N = 2$ for this system since each unit cell consists of two pendulums. Bandgaps are attenuation zones that exist between two propagation zones, and they can only exist in nonhomogeneous periodic structures. If $\alpha = \beta$, then no bandgaps will exist. An example of a system with no bandgaps can be see in Fig. 13.2a, while Fig. 13.2b provides an example of a system with a bandgap. For frequencies in the bandgap region, traveling waves will attenuate instead of propagate. For a bistable system, Eq. (13.6) must be solved for both equilibria in order to determine both bandgap profiles. For practical applications it is necessary to convert the dimensionless frequencies into dimensional frequencies using the following scaling convention: $\omega = \tilde{\omega}\sqrt{g/L}$.

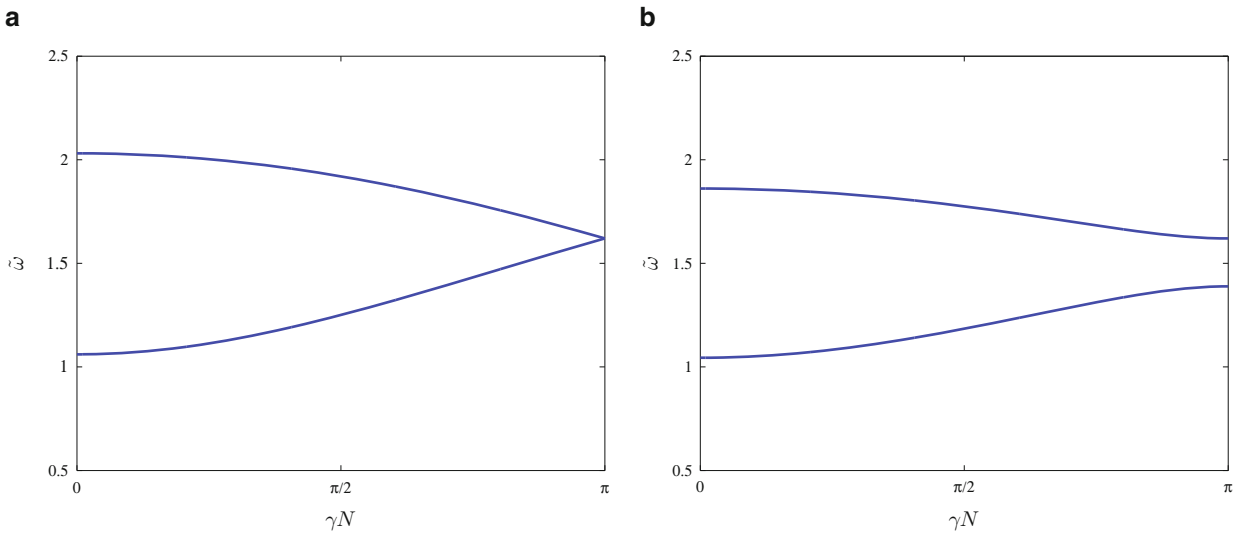

Fig. 13.2 For both of these plots, propagation zones are represented by the frequency ranges where solutions (*lines*) exist, and attenuation zones are represented by the frequency ranges where solutions do not exist (*blank space*). Plot (**a**) shows the homogeneous case where $\alpha = \beta = 1$ and no bandgaps exist. Instead, a single propagation zone exists for $1.06 < \tilde{\omega} < 2.03$. Plot (**b**) shows the existence of a bandgap region between the two propagation zones at $1.04 < \tilde{\omega} < 1.39$ and $1.62 < \tilde{\omega} < 1.86$ when $\alpha = 1$ and $\beta = 2$. For both plots, $\epsilon = 1$, $\kappa = 1$, and $\sigma = 0$. Bistability has not yet been introduced to the system, so there is only one bandgap profile for a given set of parameters

13.3 Experimental System

This section describes a set of experiments that were used to demonstrate the phenomenon of reconfigurable bandgaps. An experimental system consisting of 14 axially aligned pendulums was built, and can be seen in Fig. 13.3. The pendulums were torsionally coupled to each other using elastic bands, and magnetic interactions were used to generate the nonlinear restoring torques necessary for creating a bistable system. The system parameters were selected so that the bistability was asymmetric, resulting in two distinct bandgap profiles for the system. The first pendulum was connected to a vertical shaker that was used to excite the system, and a coupling mechanism was used to convert the translational input into a rotational input. Frequency sweeps were used to verify the two distinct bandgap profiles, and the experimental results closely matched the theoretically predicted system behavior. An amplitude sweep was then used to demonstrate amplitude dependent filtering through passive bandgap reconfiguration, and the system successfully transitioned from one bandgap configuration to the other during the experiment after an amplitude threshold was passed.

13.3.1 Bandgap Predictions

Bistability was introduced to the system through magnetic interactions. For each unit cell, a cylindrical magnet was attached to the rod of the second pendulum as the added mass (m_2). No additional mass was added to the first pendulum ($m_1 = 0$). Additional magnets were placed on a platform below the second pendulum in each unit cell, and the magnets were oriented in such a way so that they produced a repulsive magnetic force. The platforms were arranged so that they induced an asymmetric bistability in the system. The nonlinear restoring torque $f(\theta_2)$ that was created by the magnetic interactions was calculated analytically using a magnetic dipole model and numerically verified using COMSOL [16]. A plot of the potential energy for a unit cell can be seen in Fig. 13.4a. The potential energy function is the sum of the magnetic potential energy and gravitational potential energy for the system, and the placement of the magnetic platforms was manipulated to ensure that the system was asymmetrically bistable. The resulting bandgap profiles for the system can be seen in Fig. 13.4b. It can be clearly seen that the shallow well has a propagation zone in the same frequency range that the deep well has an attenuation zone. This is an important property of the system, as it enables amplitude dependent filtering.

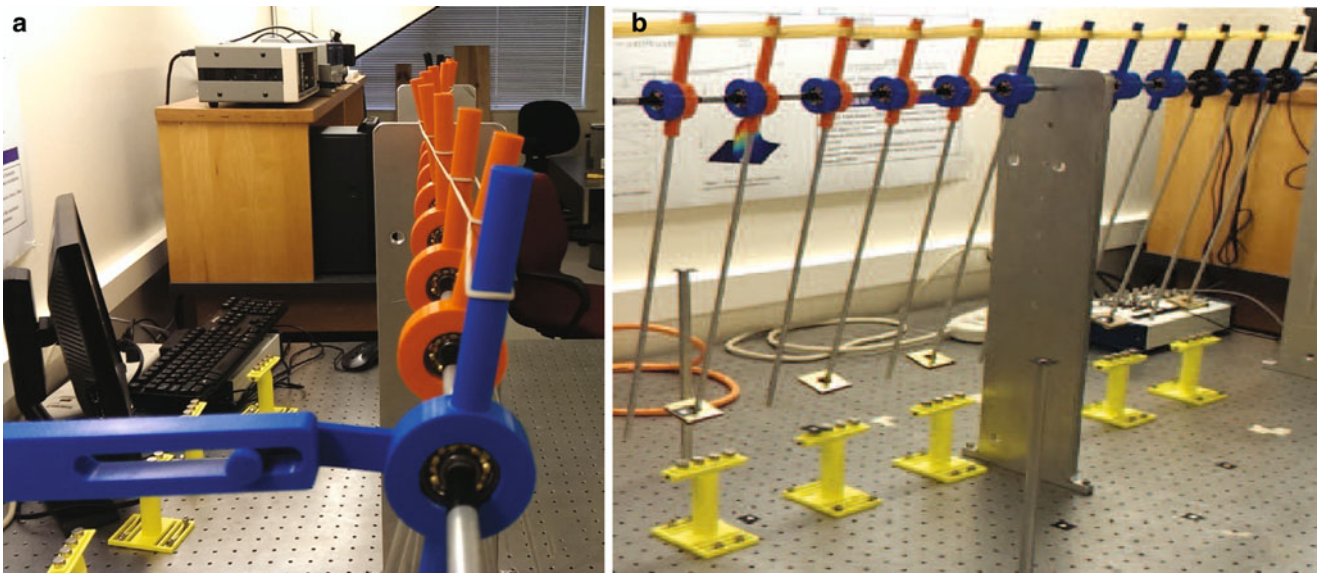

Fig. 13.3 Photographs of the experimental setup. Photo (**a**) shows the coupling mechanism that converts the translational motion of the shaker into a rotational input to the system. Photo (**b**) shows the pendulums in the shallow well configuration. The experimental system has the following parameter values: $m = 0.0347\,\text{kg}$, $m_1 = 0$, $m_2 = 0.0807\,\text{kg}$, $L = 0.4250\,\text{m}$, and $\epsilon = 0.9412$. In the shallow well, $k = 0.4203\,\text{Nm/rad}$ and $\sigma = 6.1219$. In the deep well, $k = 0.4033\,\text{Nm/rad}$ and $\sigma = 0.9083$. The stiffness values were obtained experimentally from the elastic bands used to couple the pendulums, and the values are slightly different for the two cases due to a nonlinear relationship between coupling strength and displacement. However, for inter-well behavior the coupling can be considered linear since the angular displacements are relatively small

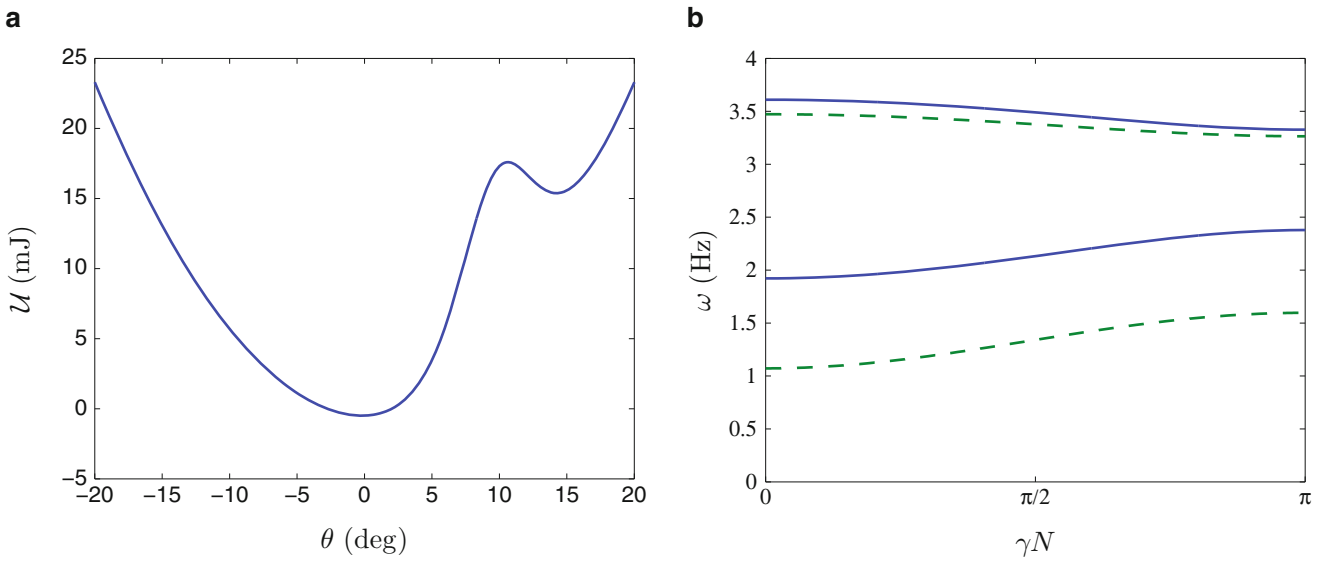

Fig. 13.4 Plot (**a**) shows the asymmetric potential energy function of a unit cell, where $\mathcal{U}$ is the potential energy of the system. Notice that there is a deep well and a shallow well. Plot (**b**) shows the bandgap profiles for the two wells. The shallow well (*solid blue lines*) has a bandgap region between the two propagation zones at 1.92 Hz $< \omega <$ 2.38 Hz and 3.33 Hz $< \omega <$ 3.61 Hz, while the deep well (*dashed green line*) has a bandgap region between the two propagation zones at 1.07 Hz $< \omega <$ 1.60 Hz and 3.26 Hz $< \omega <$ 3.47 Hz. Note that the shallow well has a propagation zone in the same frequency range that the deep well has an attenuation zone (Color figure online)

13.3.2 Frequency Sweeps

Frequency sweeps were conducted to verify the bandgap structures predicted in Fig. 13.4b. For each well, a forward and reverse frequency sweep was performed. Video capture technology was used to determine the angular displacements of the pendulums during the frequency sweeps [16]. The results of these frequency sweeps for all oscillators can be seen in Fig. 13.5, which clearly shows that two distinct propagation zones exist in each well, with a bandgap region in between. In Fig. 13.6, the response of the fifth oscillator is analyzed for each frequency sweep to verify that the system's bandgap structure matches the theoretically predicted propagation and attenuation zones. The fifth oscillator was arbitrarily selected for this analysis, and it can be seen from Fig. 13.5 that its behavior matches the behavior of the other oscillators.

13.3.3 Amplitude Sweep

An amplitude sweep was used to demonstrate amplitude dependent filtering through passive bandgap reconfiguration. The pendulums were placed in the shallow well configuration, and the excitation frequency was set to 2.1 Hz, which falls in the propagation zone for the shallow well and the bandgap region of the deep well, as seen in Fig. 13.4b. The excitation amplitude was then slowly ramped up. After approximately 160 s, a bifurcation occurred and the pendulums escaped from the shallow well into the deep well, and the system reconfigured its bandgap properties. It took approximately 1 min for transient effects to fade away, but then the amplitude of oscillations for the pendulums was almost zero, even though the excitation amplitude was still increasing. This experiment successfully demonstrates amplitude dependent filtering through passive bandgap reconfiguration, and the experimental results can be seen in Fig. 13.7. Plot (a) analyzes the response of the fifth oscillator and clearly demonstrates that the system's behavior switched from propagation to attenuation after the bifurcation occurred and transient effects settled down. Plot (b) verifies that the excitation amplitude was steadily increasing throughout the experiment. Plot (c) shows that all of the pendulums transitioned from the shallow well to the deep well nearly simultaneously. Video capture technology was used to determine the angular displacements of the pendulums during the amplitude sweep [16]. This experiment successfully demonstrated amplitude dependent filtering, as waves were allowed to propagate through the system as long their amplitude was below the bifurcation threshold. After crossing the threshold, passive bandgap reconfiguration occurred and waves were attenuated instead of propagated through the system.

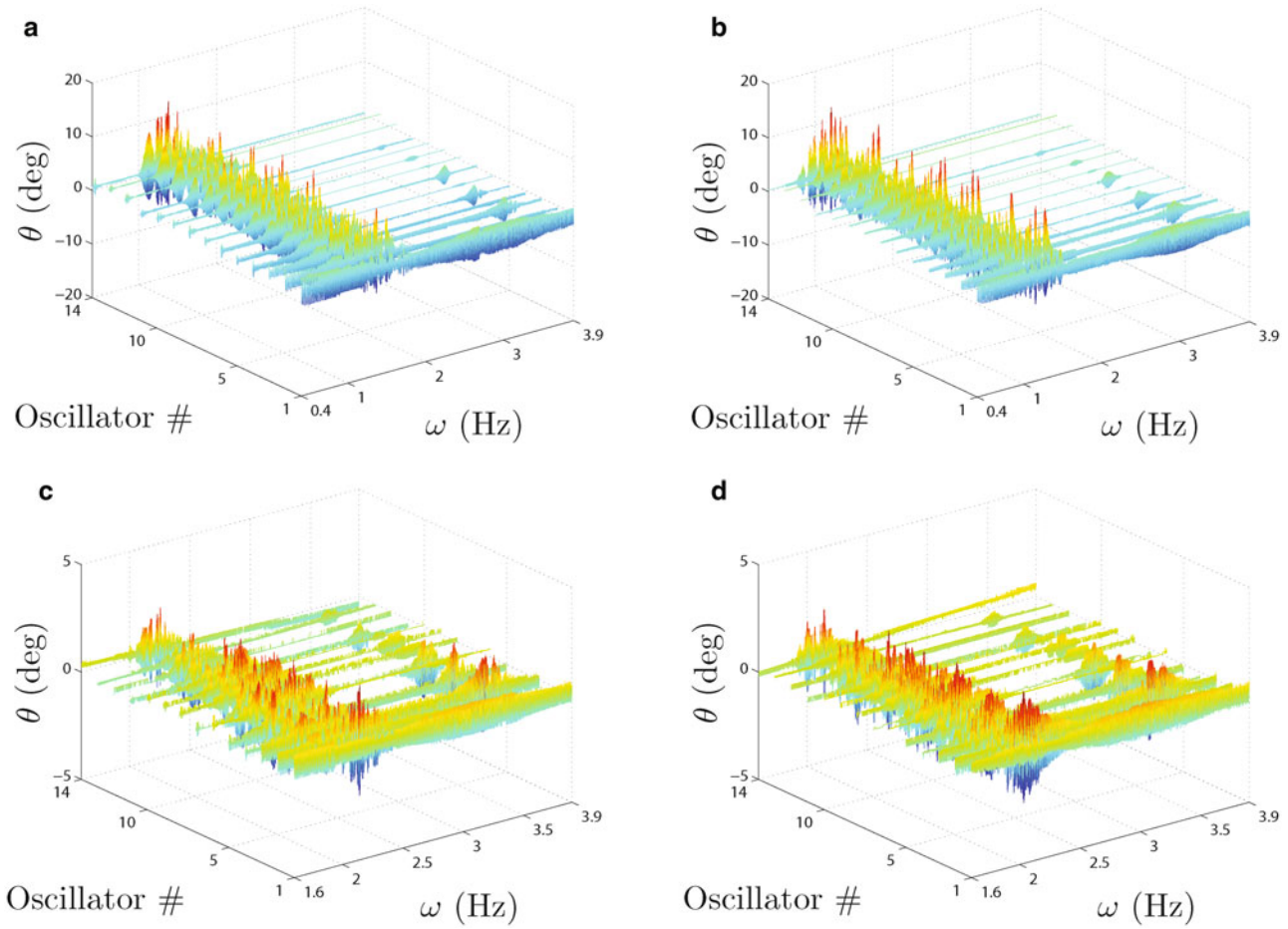

Fig. 13.5 These plots show the experimental results of various frequency sweeps in the pendulum assembly, and it can be seen that two distinct propagation zones exist in each well, with a bandgap region in between. Plot (**a**) shows the forward frequency sweep for the deep well, plot (**b**) shows the reverse frequency sweep for the deep well, plot (**c**) shows the forward frequency sweep for the shallow well, and plot (**d**) shows the reverse frequency sweep for the shallow well. The first oscillator behaves differently from the rest because it is being directly driven by the vertical shaker. The last oscillator also behaves slightly differently due to boundary effects

13.4 Conclusion

This paper presents a mathematical model that describes the bandgap structure for a 1D chain of bistable oscillators, and shows that introducing an asymmetric bistability into the system will result in two distinct bandgap structures. Bandgaps are attenuation zones that exist between two propagation zones, and it is often desirable to tune these bandgaps for specific applications. This paper shows that the system can be tuned so that it can achieve amplitude dependent filtering through passive bandgap reconfiguration. This enables waves to propagate through the system as long their amplitude is below a critical threshold. After crossing the threshold, passive bandgap reconfiguration occurs and waves are attenuated instead of propagated through the system. An experimental system was constructed to demonstrate this phenomenon, and comparisons between experiments and theory show good agreement.

Acknowledgements The authors would like to thank Xiao Wen, Jake Greenstein, Charlie Arentzen, and Jared Little for their contributions to this project. This project was primarily funded by the NSF through grants CMMI-1300307 and CMMI-1300658, and it was also supported by the ARO.

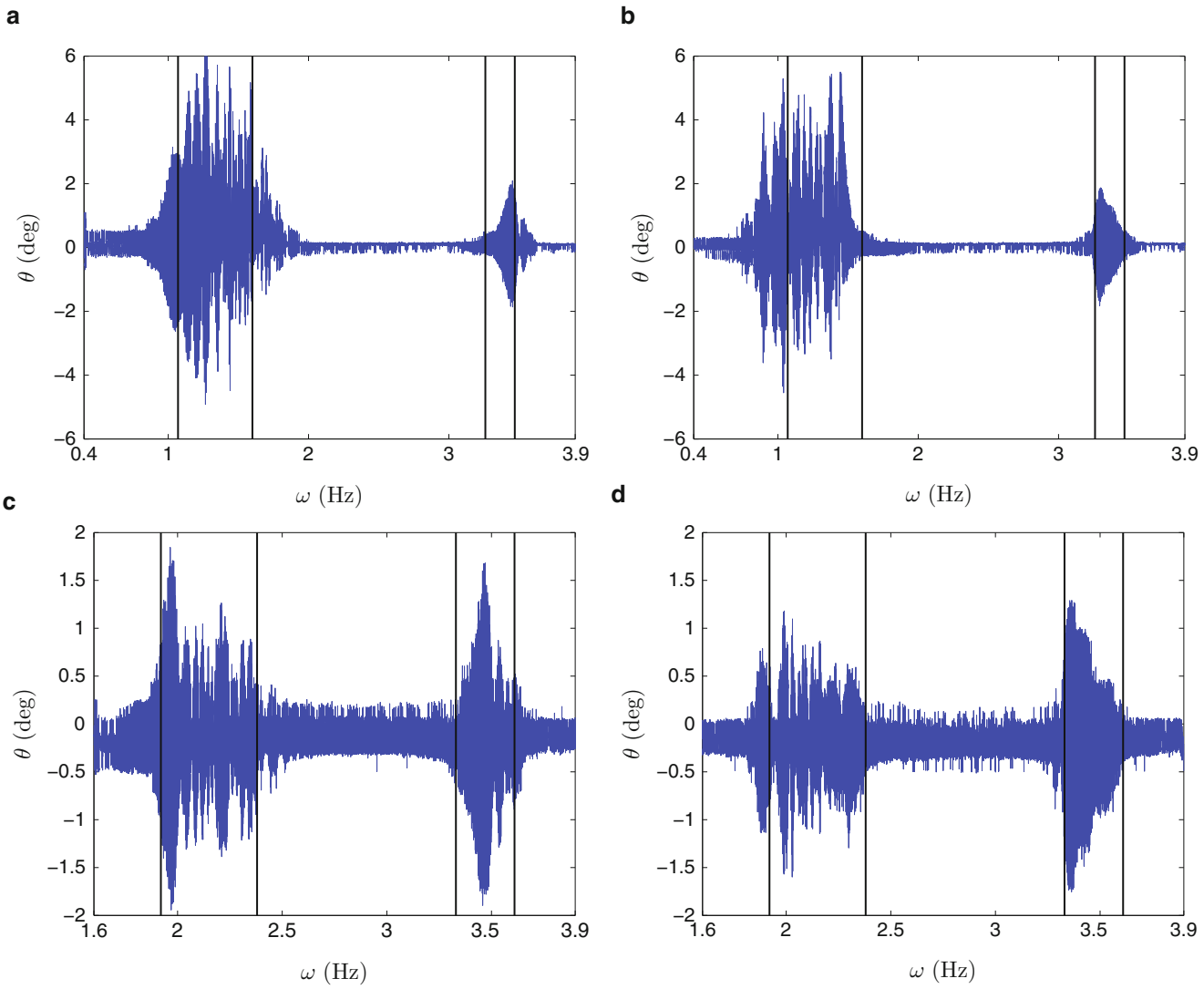

Fig. 13.6 These plots analyze the experimental response of the fifth oscillator of the pendulum assembly during various frequency sweeps, and it can be seen that the system's behavior closely matches the theoretically predicted propagation and attenuation zones. The fifth oscillator was arbitrarily selected for this analysis, and it can be seen from Fig. 13.5 that its behavior matches the behavior of the other oscillators. Plot (**a**) shows the forward frequency sweep for the deep well, plot (**b**) shows the reverse frequency sweep for the deep well, plot (**c**) shows the forward frequency sweep for the shallow well, and plot (**d**) shows the reverse frequency sweep for the shallow well. The propagation zones for the system are identified by the vertical black lines at their borders. Oscillations sometimes appear outside the propagation zones, which can be attributed to transient effects during the sweeps

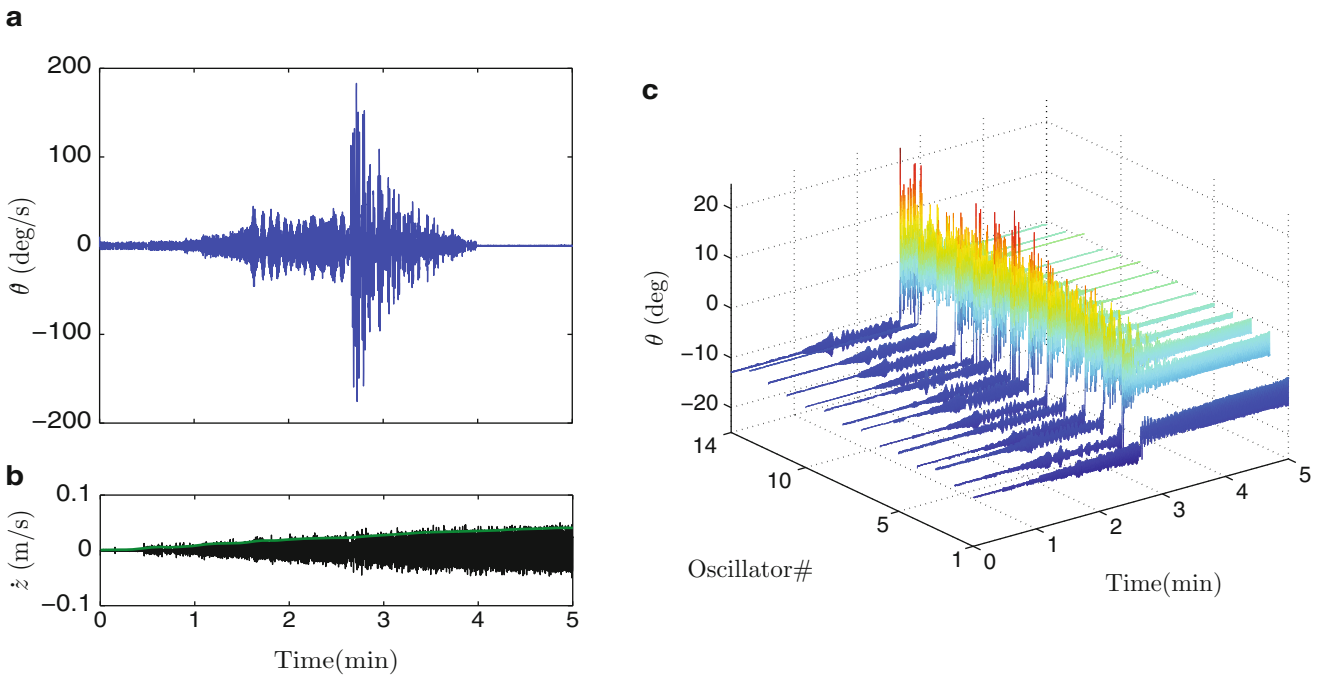

Fig. 13.7 These plots demonstrates amplitude dependent filtering through passive bandgap reconfiguration. Plot (**a**) analyzes the fifth oscillator in the pendulum assembly during an amplitude sweep, and shows how the amplitude of oscillations increases until a bifurcation occurs and the system transitions from the propagation zone in the shallow well to the attenuation zone in the deep well. After transient effects fade away, the system's oscillations are almost zero, even though the amplitude of excitation for the system is still increasing. Plot (**b**) verifies that the excitation amplitude was steadily increasing throughout the experiment ($\dot{z}$ is the velocity of the vertical shaker input). Plot (**c**) shows that all of the pendulums transitioned from the shallow well to the deep well nearly simultaneously. The first oscillator behaves differently from the rest because it is being directly driven by the vertical shaker

References

1. Friesecke G, Wattis JAD (1994) Existence theorem for solitary waves on lattices. Commun Math Phys 161:391–418
2. Lazaridi AN, Nesterenko VF (1985) Observation of a new type of solitary waves in a one-dimensional granular medium. J Appl Mech Tech Phys 26:405–408
3. Mead DJ (1996) Wave propagation in continuous periodic structures: research contributions from Southampton, 1964–1995. J Sound Vib 190:495–524
4. Brillouin L (1953) Wave propagation in periodic structures. Dover, New York
5. Kushwaha MS, Halevi P, Dobrzynski L, Djafari-Rouhani B (1993) Acoustic band structure of periodic elastic composites. Phys Rev Lett 71:2022–2025
6. Kushwaha MS, Halevi P, Martinez G, Dobrzynski L, Djafari-Rouhani B (1994) Theory of acoustic band-structure of periodic elastic composites. Phys Rev B Condens Matter Mater Phys 49:2313–2322
7. Daraio C, Nesterenko VF, Herbold EB, Jinn S (2006) Energy trapping and shock disintegration in a composite granular medium. Phys Rev Lett 96:058002
8. Zhou XZ, Wang YS, Zhang C (2009) Effects of material parameters on elastic band gaps of two-dimensional solid phononic crystals. J Appl Phys 106:014903
9. Sun HX, Zhang SY, Shui XJ (2012) A tunable acoustic diode made by a metal plate with periodical structure. J Appl Phys 100:103507
10. Doney R, Sen S (2006) Decorated, tapered, and highly nonlinear granular chain. Phys Rev Lett 97:155502
11. Zhou W, Mackie DM, Taysing-Lara M, Dang G, Newman PG, Svensson S (2006) Novel reconfigurable semiconductor photonic crystal-mems device. Solid State Electron 50:908–913
12. Edalati A, Boutayeb H, Denidni TA (2007) Band structure analysis of reconfigurable metallic crystals: effect of active elements. J Electromagn Waves Appl 21:2421–2430
13. Herbold EB, Kim J, Nesterenko VF, Wang SY, Daraio C (2009) Pulse propagation in a linear and nonlinear diatomic periodic chain: effects of acoustic frequency band-gap. Acta Mech 205:85–103
14. Yang XS, Wang BZ, Zhang Y (2004) Pattern-reconfigurable quasi-yagi microstrip antenna using a photonic band gap structure. Microw Opt Technol Lett 42:296–297
15. Bernard BP, Mann BP (2013) Passive band-gap reconfiguration born from bifurcation asymmetry. Phys Rev E Stat Nonlinear Soft Matter Phys 88:052903
16. Bernard BP, Mazzoleni MJ, Garraud N, Arnold DP, Mann BP (2014) Experimental investigation of bifurcation induced bandgap reconfiguration. J Appl Phys 116:084904
17. Jensen JS (2003) Phononic band gaps and vibrations in one- and two-dimensional mass-spring structures. J Sound Vib 266:1053–1078